HOKKAIDO UNIVERSITY

Title	Matrix sublimation method for the formation of high-density amorphous ice
Author(s)	Kouchi, A.; Hama, T.; Kimura, Y. et al.
Citation	Chemical physics letters, 658, 287-292 https://doi.org/10.1016/j.cplett.2016.06.066
Issue Date	2016-06-24
Doc URL	https://hdl.handle.net/2115/70840
Rights	©2016, Elsevier. This manuscript version is made available under the CC-BY-NC-ND 4.0 license http://creativecommons.org/licenses/by-nc-nd/4.0/
Rights(URL)	https://creativecommons.org/licenses/by-nc-nd/4.0/
Type	journal article
File Information	Kouchi et al. CPL03.text.pdf

Hokkaido University Collection of Scholarly and Academic Papers : HUSCAP

Matrix sublimation method for the formation of high-density amorphous ice

Kouchi, A.[a]*, Hama, T.[a], Kimura, Y.[a], Hidaka, H.[a], Escribano, R.[b], & Watanabe, N.[a]

[a] Institute of Low Temperature Science, Hokkaido University, Sapporo 060-0819, Japan.

[b] Instituto de Estructura de la Materia, Consejo Superior de Investigaciones Cientificas, IEM-CSIC, 28006 Madrid, Spain.

* Corresponding author.

E-mail address: kouchi@lowtem.hokudai.ac.jp (A. Kouchi)

Graphical abstract

Highlights

- Matrix sublimation method for preparing amorphous ice has been developed.
- Amorphous ice formed exhibits a highly porous microscale texture.
- The amorphous ice is a high-density form similar to that formed at high-pressures.

Keywords: Matrix sublimation, ice, high-density amorphous ice,

ABSTRACT

A novel method for the formation of amorphous ice involving matrix sublimation has been developed. A CO-rich CO:H_2O mixed ice was deposited at 8-10 K under ultra-high vacuum condition, which was then allowed to warm. After the sublimation of matrix CO at 35 K, amorphous ice remained. The amorphous ice formed exhibits a highly porous microscale texture; however, it also rather exhibits a density similar to that of high-density amorphous ice formed under high pressure. Furthermore, unlike conventional vapor-deposited amorphous ice, the amorphous ice is stable up to 140 K, where it transforms directly to cubic ice Ic.

1. Introduction

The importance of amorphous ice is widely recognized in the fields of physics,

chemistry [1,2], and cryobiology [3], but is of particular interest in planetary science and astrophysics [4]. Various procedures for the preparation of amorphous ice have been developed in order to investigate the relationship between its structure and method of formation [2] (Fig. 1). Vapor deposition methods were often applied to prepare amorphous solid water (ASW) in a vacuum [5,6]. When water (H_2O) vapor is deposited onto a surface below 40 K, high-density ASW can be produced. In contrast, deposition at 40−70 K results in low-density ASW [6,7]. Unique property of ASW that is distinct from other amorphous ices is that ASW has larger surface area and higher porosity [8,9]. Rapid cooling of micron-sized water droplets or thin film can form amorphous ice referred to as hyperquenched glassy water (HGW) [10,11]. HGWs formed at ambient and high pressures are low- and high-density forms, respectively [12].

Disruption of ice crystals by compression or irradiation with high-energy particles is also known as formation method of amorphous ice [13-16]. High-density amorphous ice (HDA), which is distinct from the ASW and HGW formed at low pressures, could be formed by compression of ice crystals at high pressure [13,14]. HDA transforms low-density amorphous ice (LDA) by warming up at ambient pressure. Ice crystal in a

49 vacuum can be amorphized by the irradiation with high-energy electron beam [15] or
50 UV-rays at low temperature [16].

51 Since the structure of amorphous ice has been found to strongly depend on the
52 method of its formation [2,17-19] and formation conditions [2,6,7,12], as described
53 above, unknown amorphous ice structures may still be discovered through new
54 formation methods. In this letter, we report a new method for the formation of
55 amorphous ice, matrix sublimation method. Remarkably, ice prepared by sublimation of
56 a carbon monoxide (CO) matrix from a H_2O/CO mixture at around 35 K shows a highly
57 porous texture different from that of ASW, and a density similar to that of HDA
58 prepared under high pressure. This new method contributes to our understanding of the
59 structure and physical properties of amorphous ice and to the development of new
60 materials.

61

62 **2. Experimental**

63

64 Amorphous ice was prepared according to a newly developed matrix sublimation

65 method, illustrated in Fig. 2. We observed this process *in situ* using the ultra-high
66 vacuum (UHV) transmission electron microscope (TEM) and Fourier-transform
67 infrared (FTIR) spectrometry.

68 A specially designed UHV TEM (JEOL JEM-2100V) for *in situ* observation of ice
69 was developed following Kondo *et al*. [20]. Since the specimen was surrounded by a
70 liquid nitrogen shroud, the pressure around the specimen was lower than the pressure of
71 the specimen chamber (1×10^{-6} Pa). We used a liquid He cooling holder (Gatan
72 ULTST) for specimen cooling, and a 5-nm-thick amorphous Si film (SiMPore Inc.) as a
73 substrate for sample deposition. Of the three ports directed at the specimen surface, the
74 one with an incident angle of 55° was used for a Ti gas inlet tube (inner diameter = 0.4
75 mm).

76 CO was used as the matrix because it is an astrophysically important molecule,
77 active for IR spectroscopy, and could be evacuated by ion pumps equipped with a TEM.
78 Mixtures of CO and H_2O at ratios of 50:1 and 10:1 were deposited on the Si thin film at
79 about 8 K. We did not record TEM images during deposition to avoid damage from the
80 electron beam. After deposition, the sample substrate was warmed at a rate of

81 approximately 2.0 K/min, controlled manually. TEM images could not be recorded
82 during the sublimation of CO because the pressure was higher than 10^{-4} Pa. The
83 thickness of the ice samples remaining after CO sublimation was several tens of
84 nanometres. To avoid electron-beam damage to the sample, a low-dose imaging
85 technique was applied in which the accelerating voltage was 80 kV, the electron beam
86 current was less than 0.1 pA/cm^2 and low magnification images were recorded using a
87 CCD camera (Gatan ES500W). Furthermore, subsequent observations were taken from
88 different positions of the sample. The edge of a single crystalline Si grid was used for
89 the calibration of length in the analysis of the electron diffraction patterns.

90 For FTIR spectroscopy, we used a laboratory setup for surface reactions in
91 interstellar environments (LASSIE) apparatus, as described previously [21]. The
92 samples were prepared using a background deposition method on an Al substrate cooled
93 to 10 K by He refrigeration. After deposition, the sample substrate was warmed at a rate
94 of 2.0 K/min. IR spectra of samples were obtained and monitored by
95 reflection–absorption spectroscopy. Typical column density of the samples after CO
96 sublimation was 1.5×10^{16} molecules/cm^2.

3. Results and discussion

As shown in Fig. 3a, the CO:H_2O ice deposited at 8 K is a mixture of crystalline □-CO and a small amount of amorphous CO. Water molecules are embedded in the CO matrix as clusters (see Supplementary Fig. 1 and Supplementary Table 1. [22-24]). After the sublimation of CO at 25–40 K, we observed highly porous ice, as shown in Fig. 3b and Fig. 4; we term this the matrix-sublimated ice (MSI). The MSI shows wide textural variety at the micro- and submicroscale, with the ice exhibiting mainly concrete-like (Fig. 4a) or granite-like (Fig. 4c) textures, along with some minor occurrences of feather-like (Fig. 4b) or seaweed-like (Fig. 4d) textures. Conversely, these types of structures (micro- and submicroscale highly porous structures) are not observed in pure H_2O vapor-deposited amorphous ice, that is, ASW, as shown in Fig. 5. In addition, no temperature dependence on the structure of ASW was observed until crystallization occurs. However, the previous studies reported that ASW has larger surface area and higher porosity at lower temperatures, and it becomes less porous as the temperature

113 increases [8,9]. We speculate that the space scales of porous structures are different
114 between ASW (nanometer scale) and MS-HDA (micrometer scale), and the
115 magnification in the present observation by TEM is too low to explicitly observe the
116 porous structures of ASW. These results confirm that the formation of the highly porous
117 MSI observed in the present study is not due to electron beam irradiation during TEM
118 but due to intrinsic phenomena. This is further confirmed by IR measurements, in which
119 a destructive beam is not applied, as discussed later.

120 As described below, we have confirmed that the structure of our MSI is that of an
121 HDA ice, and have therefore termed it matrix-sublimated high-density amorphous
122 (MS-HDA) ice. Figure 6 shows the temperature dependence of the d-spacing in the
123 main halo for vapor-deposited ASW and MS-HDA ice. In ASW, the d-spaces of the
124 main peak increase with temperature, as observed by Jenniskens and Blake [6]. They
125 assigned the lower and higher temperature forms as high-density ASW (HD-ASW) and
126 low-density ASW (LD-ASW), respectively. Conversely, the d-spacing in the MS-HDA
127 ice does not change with temperature, and remains constant at ca. 0.31 nm irrespective
128 of whether the initial ice composition ($CO:H_2O$) is 10:1 or 50:1. Winkel *et al*. reported

129 that the d-spaces in HDA ice made by submitting ice Ih to high pressure ranged from
130 0.28 to 0.32 nm [18], and the d-spaces of 0.31 nm for MS-HDA ice fall within this
131 range. The density of MS-HDA ice is estimated to be 1.16 g/cm^3 from the relationships
132 of d-spaces with pressure (0.1 GPa) [18], and pressure with density [25,26]. Mishima *et*
133 *al*. have reported that the density of HDA ice at ambient pressure is 1.17 g/cm^3 [13].
134 Thus, we conclude that the MS-HDA ice generated in the present study is a high-density
135 form similar to HDA ice produced under high pressure, but different from HD-ASW
136 produced by vapor-deposition in a vacuum.

137 MS-HDA ice formed at around 35 K is very stable against temperature change up to
138 140 K. At temperatures around 140 K, MS-HDA ice directly transforms into ice Ic (Fig.
139 7). The transformation of HDA ice during heating depends on the initial formation
140 conditions, annealing conditions, pressure and heating rate. Consequently, different
141 transformation sequences (e.g. HDA → LDA → ice Ic and HDA → ice Ic) have been
142 observed [27-29]. Although direct comparison between MS-HDA ice and HDA ice is
143 difficult, it is worth noting that the behaviour of MS-HDA ice observed in the present
144 study resembles that of HDA ice formed at 0.1 GPa [27] rather than that formed at

145 0.001 GPa.

146 Figure 8 and Supplementary Fig. 1 show the changes in the FTIR spectra with
147 temperature for ice of three different initial CO:H_2O ratios, i.e. 50:1, 10:1 and pure H_2O
148 (ASW). A summary of the assignments is given in Supplementary Table 1. At low
149 temperatures (10 and 20 K), monomers are present in the 50:1 ice, as the ν_3 asymmetric
150 and ν_1 symmetric stretching modes of H_2O monomers are observed at 3707 cm^{-1} and
151 3617 cm^{-1}, respectively. However, no monomers are indicated in the 10:1 ice, but strong
152 absorptions due to polymeric aggregates are observed (Supplementary Table 1). During
153 the sublimation of CO around 30 K, the intensity of the water cluster bands decreases
154 suddenly, and the characteristic OH stretching band at 3000–3600 cm^{-1} of solid water
155 ice becomes stronger. After the sublimation of CO, MS-HDA ice remains. The spectral
156 characteristics of the OH stretching band clearly differ between MS-HDA ice and ASW
157 (Fig. 8). The spectral features and peak wavenumbers of MS-HDA ice made from the
158 CO:H_2O mixture at ratios of 50:1 (Figs. 8a and b) and 10:1 (Figs. 8c and d) do not
159 change with temperature, indicating the stability of MS-HDA ice. Conversely, those of
160 vapor-deposited ASW changes as the temperature increases (Figs. 8e and f) [30],

161 indicating that HD-ASW deposited at 10 K is relatively unstable. Dangling-OH bonds
162 were observed in the IR spectra of MS-HDA ice and vapor-deposited ASW
163 (Supplementary Fig. 2) [31]. These spectroscopic results imply that MS-HDA has
164 porous structures like ASW at nanometer scale, in addition to the porous structures at
165 micrometer scale as shown in Fig. 5.

166 Although we cannot precisely clarify the formation mechanism of MS-HDA ice, the
167 following rationales are presented: The Laplace pressure of a 1.0 nm radius fine particle
168 of MS-HDA ice is 0.14 GPa if we assume that its surface tension 70 mN/m. This
169 pressure is similar to the lowest pressures at which HDA ice is formed. Thus, water
170 aggregates of a few nanometres in diameter may be formed with high internal density.
171 Another possibility is that the stress in the crystalline α-CO matrix plays an important
172 role, as is acknowledged for thin films [32]. The stress in the solid could force the water
173 molecules to be segregated into high-density pores.

174 The matrix sublimation method developed in the present study is a novel means of
175 forming amorphous ice and supplements previously known methods. In vapor
176 deposition and liquid water quenching, the surface temperature of the amorphous ice

177 becomes higher owing to the heat of condensation [33] and solidification, respectively,
178 which can sometimes lead to the crystallisation. Conversely, in the matrix sublimation
179 method, the sample surface is cooled owing to the sublimation heat of the matrix. In the
180 high-pressure compression of ice crystals, transformation to amorphous ice is limited at
181 temperatures higher than 77 K, and in irradiation methods, decomposition of water
182 molecules is unavoidable. However, in the matrix sublimation method, no
183 decomposition of water molecules occurs, and there is no temperature limit if we
184 choose a suitable matrix species.

185 It may be possible to easily make other amorphous and crystalline ices that usually
186 require a wide pressure range using modifications of the present matrix sublimation
187 method with, for example, various ratios of matrix to water, various types of matrix (i.e.
188 those formed at different sublimation temperatures or with different polarity materials),
189 and various matrix sublimation rates. To explore the effect of the matrix to water ratio,
190 we performed experiments using ices formed at CO:H_2O ratios of 10:1, 50:1 and 2:1,
191 and ASW. A comparison of the d-spacing in the MSIs prepared using these ratios is
192 presented in Supplementary Fig. 3. It is clear that the size of the d-spaces in the MSI

prepared using a CO:H_2O ratio of 2:1 lies between those of MS-HDA ice and ASW, suggesting that the MSI prepared using the 2:1 ratio is a mixture of MS-HDA ice and ASW. We also performed experiments using N_2 for the matrix instead of CO, and similar results are obtained, although the d-spaces are slightly larger (Supplementary Fig. 4). These results clearly indicate that the interaction between the water and matrix molecules plays an essential role in determining the structure of the ice formed.

The most prominent feature of the matrix sublimation method is that high-pressure phases are formed very easily in a vacuum, whereas highly energetic processes such as ionization or high-temperature heating are required for other low-pressure syntheses, such as those of diamond or cubic boron nitride. Furthermore, this method may be applied to prepare other crystalline and amorphous solids. In fact, any laboratory that currently performs matrix isolation spectroscopy could also perform matrix sublimation preparation, as the apparatus needed for these techniques is essentially the same. Consequently, rapid progress in research into the formation of new materials is now possible.

4. Astrophysical implications

This study also has astrophysical implications, as CO-rich ices have been observed in icy grains within interstellar molecular clouds [34]. These grains consist of a silicate core, an inner mantle of organic refractory material, H_2O-rich amorphous ice, and a CO-rich outer mantle [35]. When CO sublimes due to the slight temperature increase during the formation of protoplanetary disks, highly porous MS-HDA ice is formed. The high porosity of icy grains could have a significant effect on the aggregation of interstellar grains and the physical properties of planetesimals. Therefore, the thermal conductivity of cometary nuclei might be smaller than has been thitherto thought [33]. Furthermore, the high porosity characteristics of cometary nuclei as observed by the Rosetta mission [36] could be explained by the aggregation of highly porous MS-HDA-covered icy grains. CO or N_2-rich ices are also observed on the surface of dwarf planets and icy satellites [37,38]. If CO or N_2 sublimes from these ices upon slight temperature increase, highly porous MS-HDA ice might be formed on the surface of these bodies.

References

[1] V.F. Petrenko, R.W. Whitworth, Physics of Ice. Oxford Univ. Press, 1999.

[2] C.A. Angell, Ann. Rev. Phys. Chem. 55 (2004) 559.

[3] A. Cavalier, D. Spehner, B.M. Humbel, eds. Handbook of Cryo-Preparation Methods for Electron Microscopy. CRC Press, 2009.

[4] R.M.E. Mastrapa, W.M. Rundy, M.S. Gudipati, In: The Science of Solar System Ices (eds. M.S. Gudipati, J.Castillo-Rogez) p371 Springer, 2013.

[5] E.F. Burton, W.F. Oliver, Proc. R. Soc. Lond. A153 (1935) 166.

[6] P. Jenniskens, D.F. Blake, Science 265 (1994) 753.

[7] A.H. Narten, C.G. Vekatesh, J.A. Rice, J. Chem. Phys. 64 (1976) 1106.

[8] E. Mayer, R. Pletzer, Nature 319 (1986) 298.

[9] K.P. Stevenson, G.A. Kimmel, Z. Dohnalek, R.S. Smith, B.D. Kay, Science 283 (1999) 1505.

[10] P. Brüggeller, E. Mayer, Nature 288 (1980) 569.

241 [11] J. Dubochet, A.W. McDowell, J. Microsc. 124 (1981) RP3.

242 [12] O. Mishima, Y. Suzuki, J. Chem. Phys. 115 (2001) 4199.

243 [13] O. Mishima, L.D. Calvert, E. Whalley, Nature 310 (1984) 393.

244 [14] T. Loerting, C.G. Salzmann, I. Kohl, E. Mayer, A. Hallbrucker, Phys. Chem. Chem.

245 Phys. 3 (2001) 5355.

246 [15] J. Lepault, R. Freeman, J. Dubochet, J. Microsc. 132 (1983) RP3.

247 [16] A. Kouchi, T. Kuroda, Nature 344 (1990) 134.

248 [17] O. Mishima, H.E. Stanley, Nature 396 (1998) 329.

249 [18] K. Winkel, M.S. Elsaesser, E. Mayer, T. Loerting, J. Chem. Phys. 128 (2008)

250 044510.

251 [19] C.A. Angel, Science 319 (2008) 582.

252 [20] Y. Kondo, K. Ohi, Y. Ishibashi, H. Hirano, Y. Harada, K. Takayanagi,

253 Ultramicroscopy 35 (1991) 111.

254 [21] N. Watanabe, T. Shiraki, A. Kouchi, Astrophys. J. Lett. 588 (2003) L121.

255 [22] W. Hagen, A.G.G.M. Tielens, J.M. Greenberg, Chem. Phys. 56 (1981) 367.

256 [23] A. Givan, A. Loewenschuss, C.J. Nielsen, J. Chem. Soc. Faraday Trans. 92 (1996)

257 4927.

258 [24] A. Givan, A. Loewenschuss, C.J. Nielsen, Vib. Spectrosc. 16 (1998) 85.

259 [25] C.G. Salzmann, T. Loerting, S. Klotz, P.W. Mirwald, A. Hallbrucker, E. Mayer,

260 Phys. Chem. Chem. Phys. 8 (2006) 386.

261 [26] T. Loerting, C.G. Salzmann, K. Winkel, E. Mayer, Phys. Chem. Chem. Phys. 8

262 (2006) 2810.

263 [27] O. Mishima, J. Chem. Phys. 100 (1994) 5910.

264 [28] P.H. Handle, M. Seidl, T. Loeting, Phys. Rev. Lett. 108 (2012) 225901.

265 [29] M. Seidl, K. Amann-Winkel, P.H. Handle, G. Zifferer, T. Loerting, Phys. Rev. B 88

266 (2013) 174105.

267 [30] W. Hagen, A.G.G.M. Tielens, J.M. Greenberg, Chem. Phys. 56 (1981) 367.

268 [31] V. Buch, J.P. Devlin, J. Chem. Phys. 94 (1991) 4091.

269 [32] F. Spaepen, Acta Mater. 48 (2000) 31.

270 [33] A. Kouchi, J.M. Greenberg, T. Yamamoto, T. Mukai, Astrophys. J. Lett. 388 (1992)

271 L73.

272 [34] W.F. Thi, K.M. Pontoppidan, E.F. van Dishoeck, E. Dartois, L. d'Hendecourt,

Astron. Astrophys. 394 (2002) L27.

[35] M. Spaans, P. Ehrenfreund, In: *Laboratory Astrophysics and Space Research*, eds. P. Ehrenfreund, K. Krafft, H. Kochan, V. Pirronello, Kluwer Academic Publisher, p. 1 (1999).

[36] W. Kofman, et al. Science 349 (2015) aab0639-1.

[37] T.C. Owen, T.L. Roush, D.P. Cruikshank, J.L. Elliot, L.A. Young, C. de Bergh, B. Schmitt, T.R. Geballe, R.H. Brown, M.J. Bartholomew, Science 261 (1993) 745.

[38] W.M. Grundy, L.A. Young, J.A. Stansberry, M.W. Buie, C.B. Olkin, E.F. Young, Icarus 205 (2010) 594.

Ackowledgements

We thank O. Mishima for critical reading of the manuscript, and S. Nakatsubo, K. Fujita, K. Sinbori and M. Ikeda for their help in the development of UHV-TEM. This study was supported by the Grant for the Joint Research Program of the Institute of Low Temperature Science, Hokkaido University, I-link-1027 project from CSIC, JSPS KAKENHI (Grant Number 25247086), and MEXT KAKENHI (Grant Number

289 25108002).

290

291

292 Figure captions

293

294 **Figure 1.** Temperature-density diagram schematic of the formation of amorphous ices.
295 The starting materials are shown in rounded rectangles, formation routes as arrows with
296 names of methods, and products in rectangles. T_g is the glass transition temperature.
297 HD-ASW, high-density amorphous solid water; LD-ASW, low-density amorphous solid
298 water; HGW, hyperquenched glassy water; HDA, high-density amorphous ice; HD,
299 high density; LD, low density; MS-HDA, matrix-sublimated high-density amorphous
300 ice; Ih, hexagonal ice.

301

302 **Figure 2**. Matrix sublimation method. Deposition of CO:H_2O on an 8–10 K substrate in
303 an ultra-high vacuum chamber. After deposition, the substrate is warmed at a constant
304 rate. Sublimation of matrix CO at 25–40 K. Formation of MSI at T > 40 K.

305

306 **Figure 3.** Low-magnification TEM image and corresponding electron diffraction

307 pattern of initial CO:H_2O=10:1 ice at 8 K (a), and MS-HDA at 80 K (b). Electron

308 diffraction pattern was obtained from the central circle region of 0.6 μm diameter.

309

310 **Figure 4.** Textural variety in highly porous MS-HDA ice. Generally, the black part is

311 thicker and white part thinner. (a, b) Initial CO:H_2O = 50:1. (c, d) Initial CO:H_2O = 10:1.

312 (Observation temperatures: a, 43 K; b, 36 K; c, 87 K; and d, 34 K.)

313

314 **Figure 5.** Low-magnification TEM image and corresponding electron diffraction

315 pattern of vapor-deposited ASW at 10 K.

316

317 **Figure 6.** Temperature dependence of d-spacing in the main halo of the electron

318 diffraction patterns of amorphous ices. ASW (orange circles) and MS-HDA ice (blue

319 squares: CO:H_2O = 10:1, green diamonds: CO:H_2O = 50:1).

320

Figure 7. Transformation from MS-HDA to ice Ic. Low-magnification TEM image and corresponding electron diffraction pattern of MS-HDA ice and ice Ic at 136 K.

Figure 8. Reflection–absorption IR spectra at different temperatures. (a, b) Initial composition of $CO:H_2O = 50:1$. (c, d) Initial composition of $CO:H_2O = 10:1$. (e, f) Pure H_2O. b, d, and f show the change in the OH stretching bands between 10 and 50 K.

Supplementary Data

Table 1. Assignment of water clusters in CO matrix.

Figure 1. Spectral change of water clusters in $CO:H_2O$ ices from 10 to 30 K. (a) Initial $CO:H_2O = 50:1$. (b) Initial $CO:H_2O = 10:1$. Wavenumbers marked by dotted lines are the same as those in Supplementary Table 1. Red and blue lines indicate monomers and polymers, respectively.

Figure 2. Reflection–absorption IR spectra at 50 K. (a) Initial composition of CO:H_2O = 50:1. (b) Initial composition of CO:H_2O = 10:1. (c) Vapor-deposited H_2O (ASW). Peaks at 3698 and 3696 cm^{-1} indicate dangling-OH bonds.

Figure 3. Temperature dependence of the d-spacing in the main halo of the electron diffraction patterns of amorphous ices made from CO:H_2O = 2:1 (yellow triangles). Grey symbols (circles, diamonds and squares) are the same data as presented in Fig. 5.

Figure 4. Temperature dependence of the d-spacing in the main halo of the electron diffraction patterns of MS-HDA ice (blue stars: N_2:H_2O = 10:1; green hexagons: N_2:H_2O = 50:1). Grey symbols (circles, diamonds and squares) are the same data as in Fig. 5.

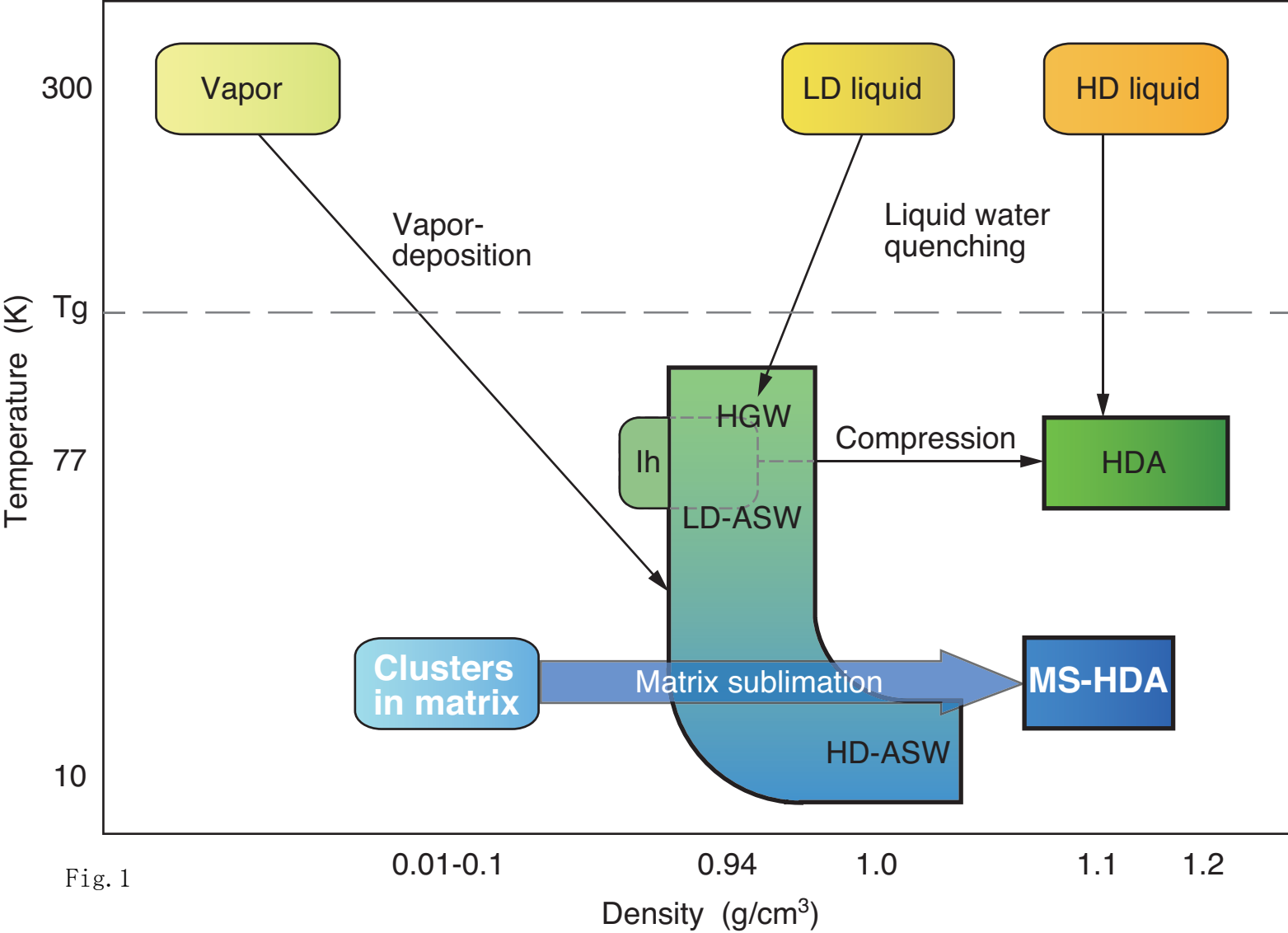
Vapor
LD liquid
HD liquid
Vapor-
deposition
Liquid water
quenching
300
Tg
77
10
Temperature (K)
HGW
Ih
LD-ASW
Compression
HDA
Clusters
in matrix
Matrix sublimation
MS-HDA
HD-ASW
0.01-0.1
0.94
1.0
1.1
1.2
Density (g/cm3)

Fig. 1

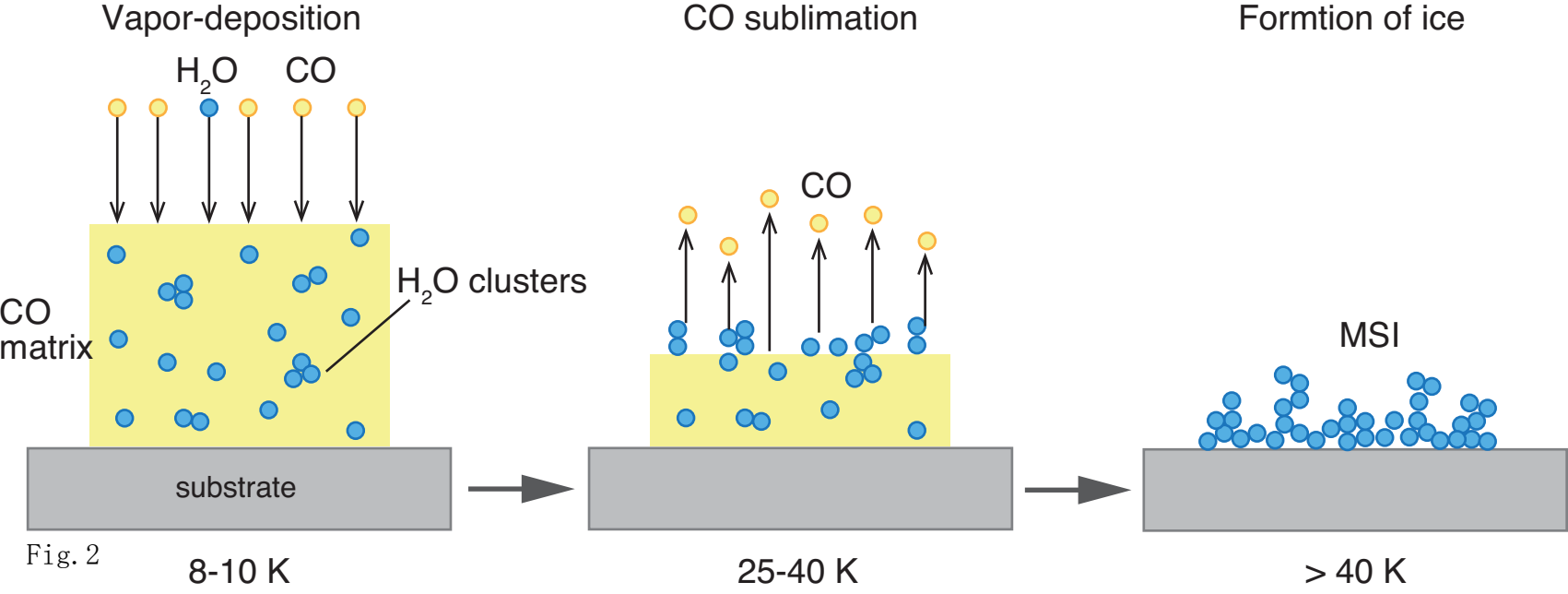
Vapor-deposition
CO sublimation
Formtion of ice
H2O
CO
CO
matrix
H2O clusters
CO
MSI
substrate
8-10 K
25-40 K
> 40 K

Fig. 2

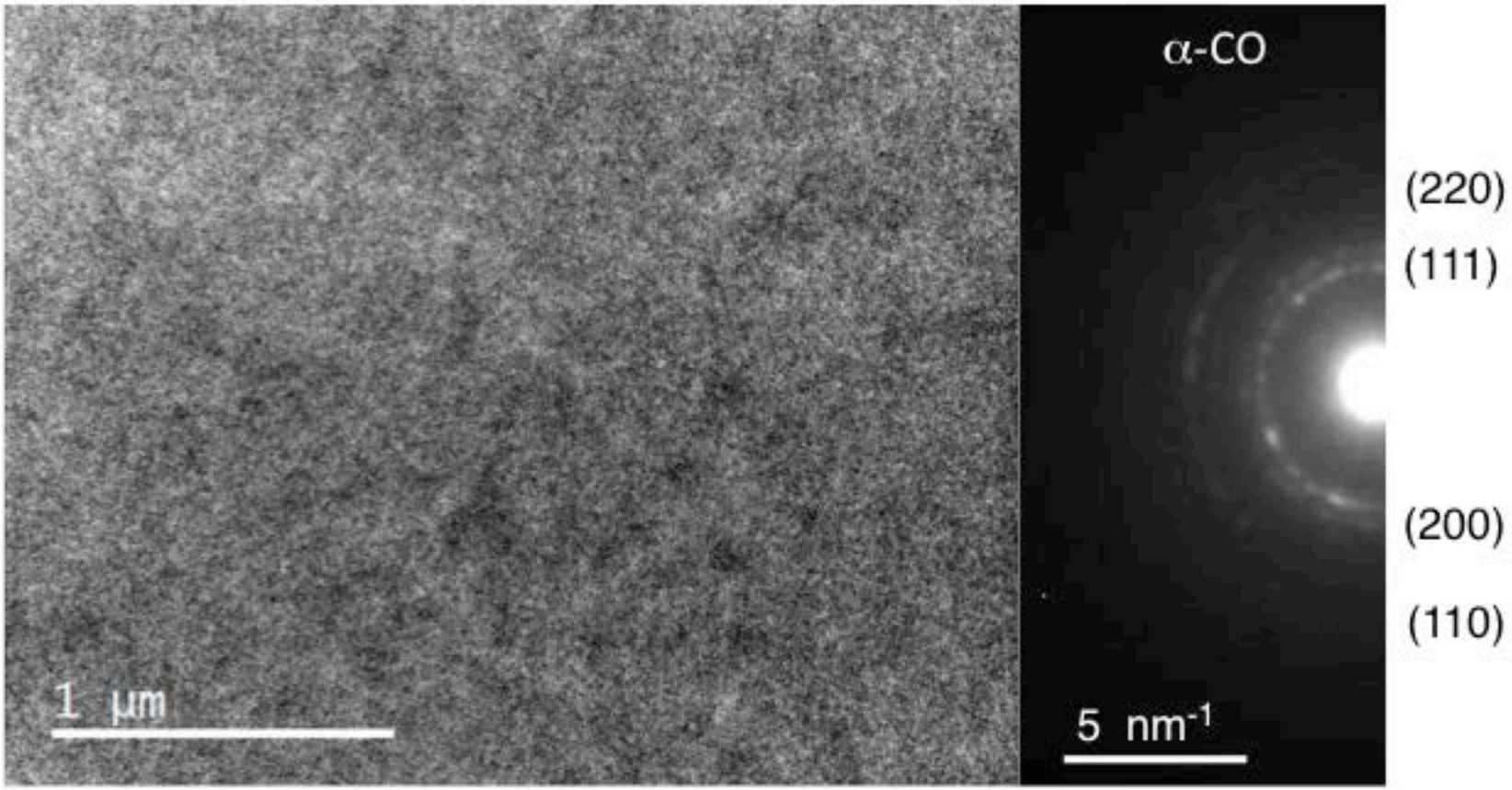

Fig.3a

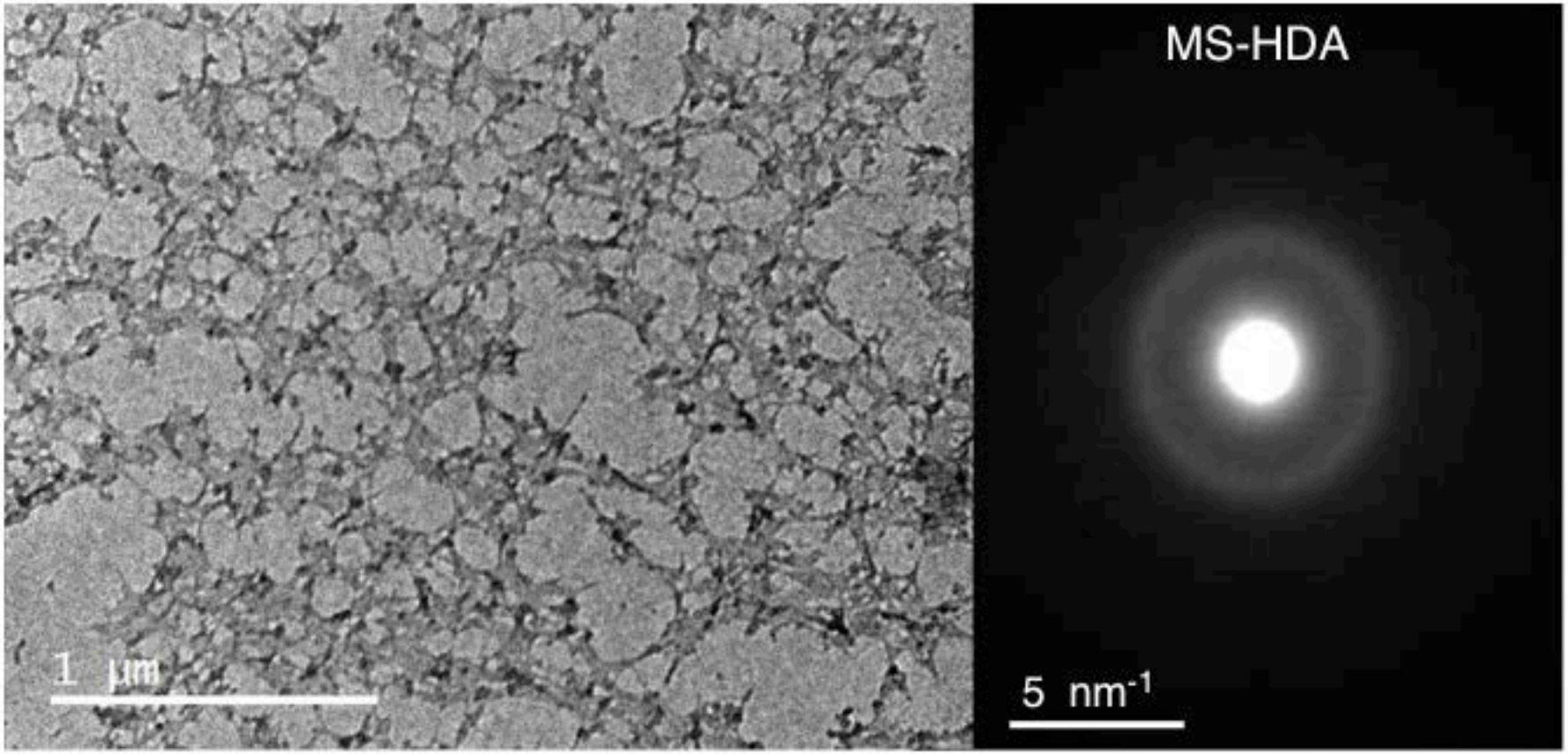

Fig. 3b

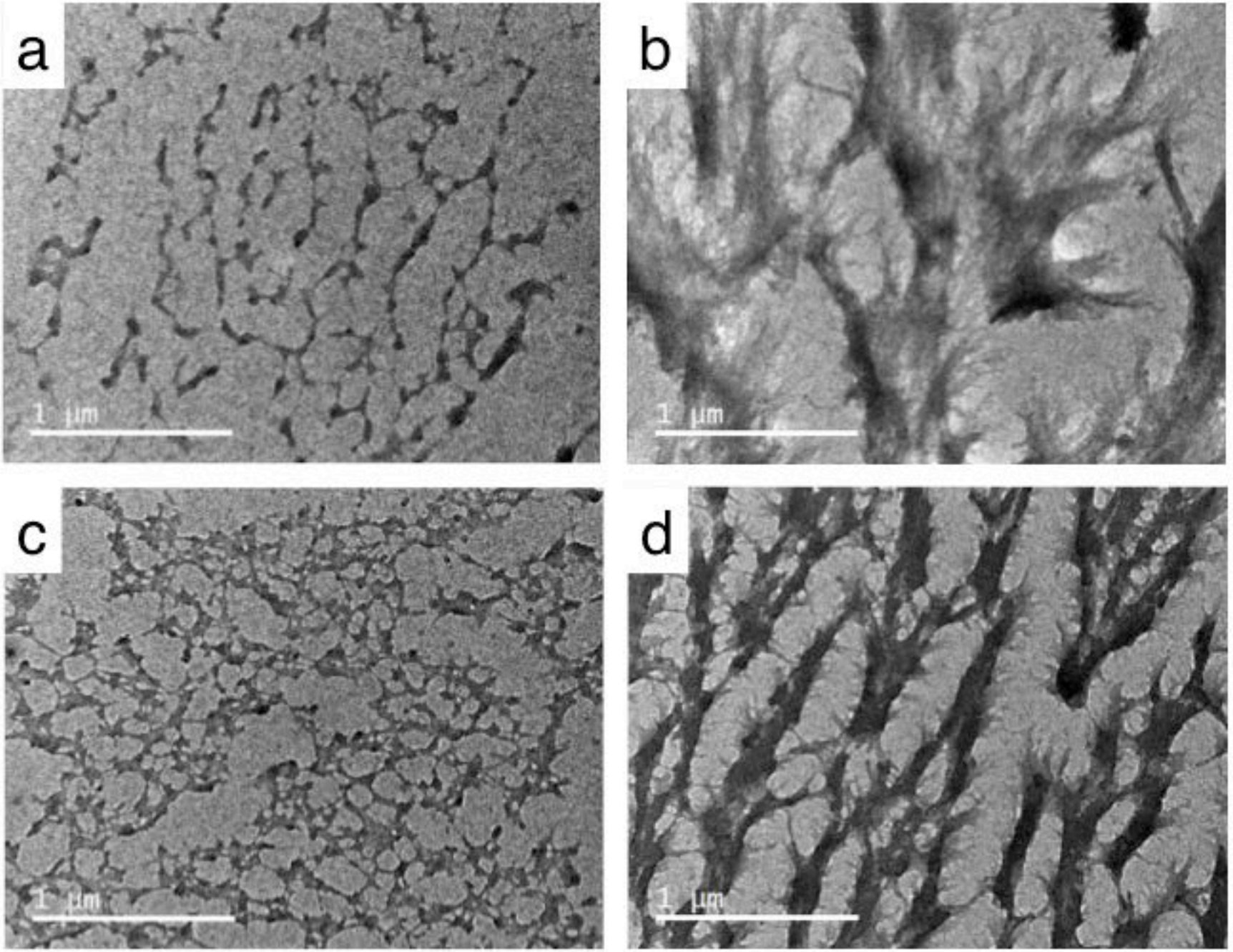

Fig. 4

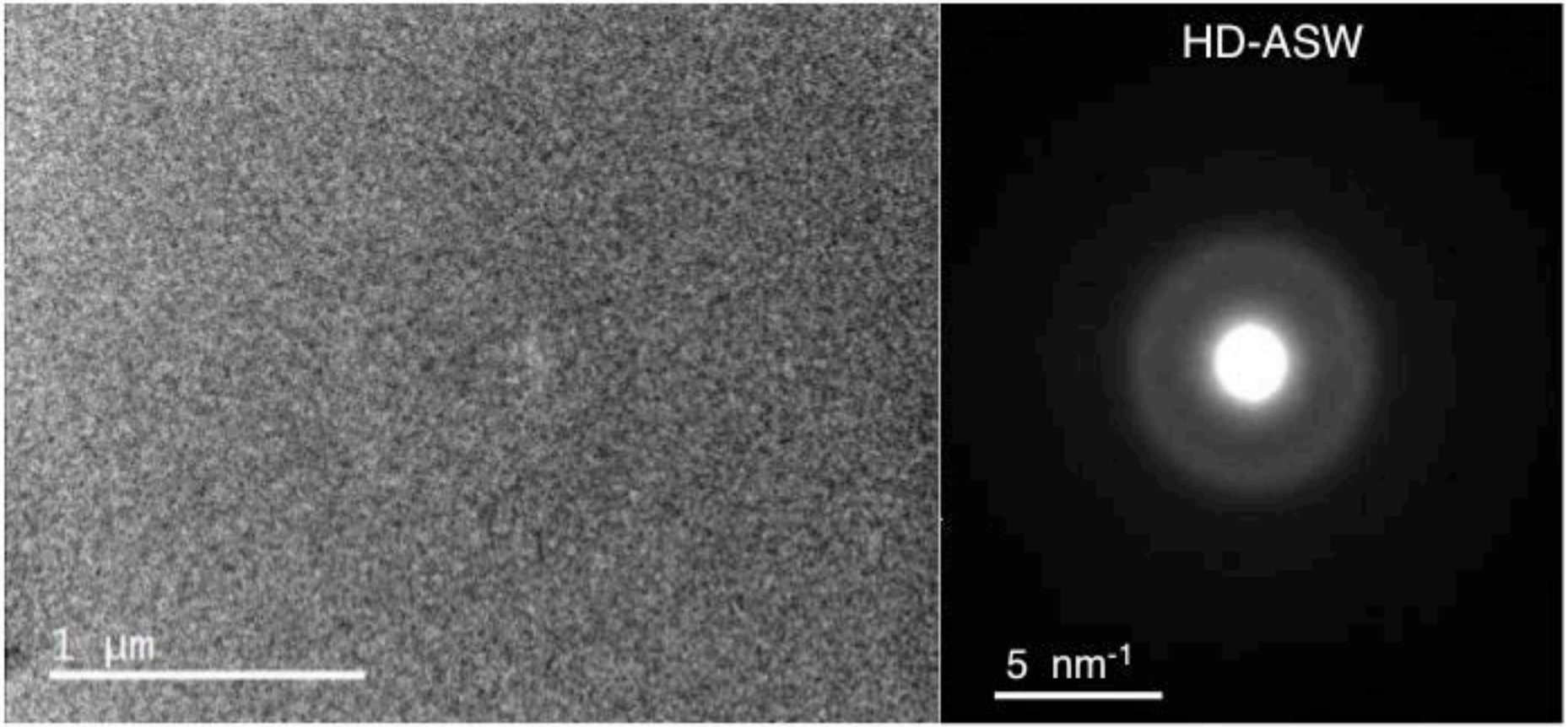

Fig.5

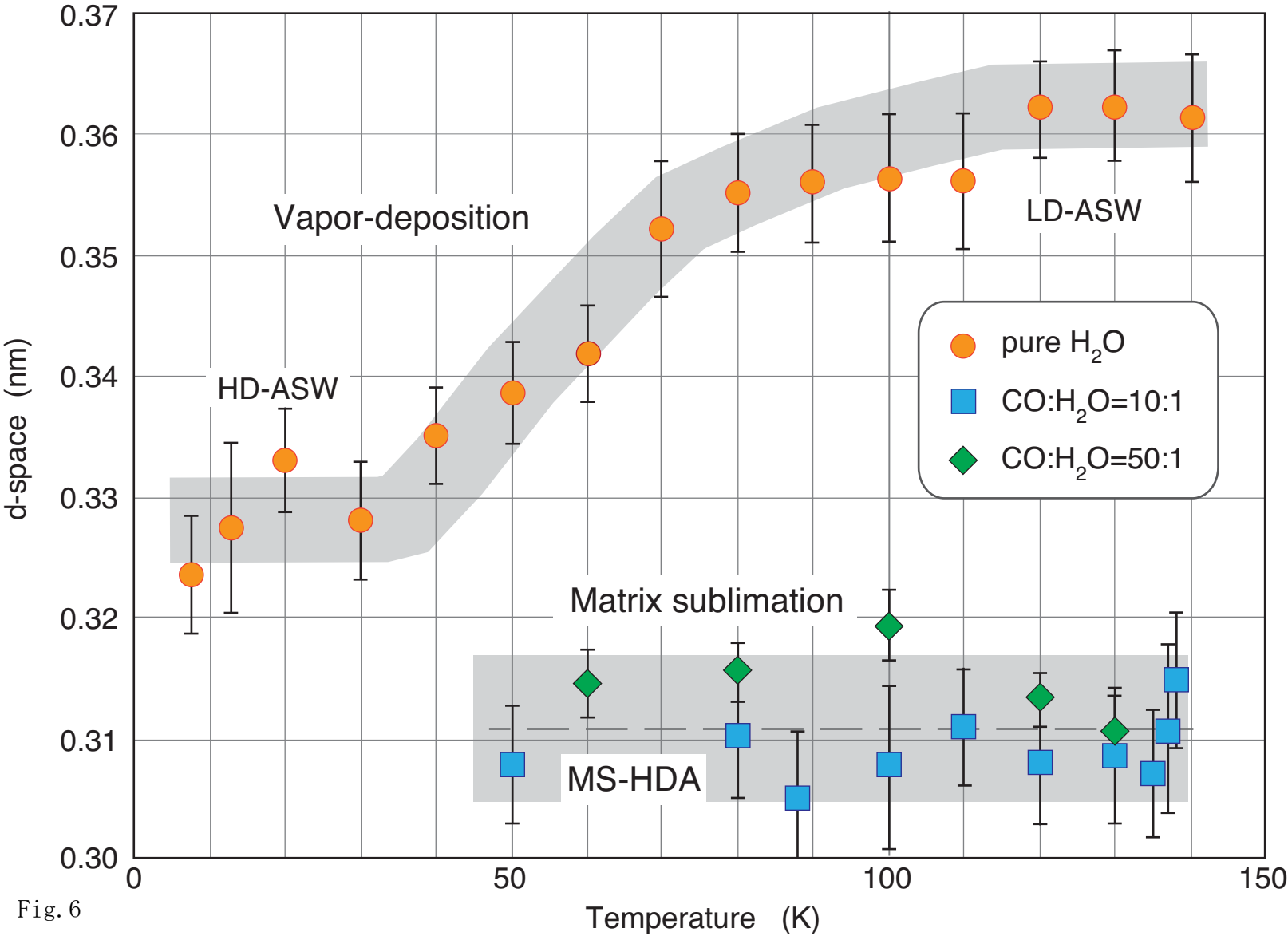
0.37
0.36
0.35
0.34
0.33
0.32
0.31
0.30
d-space (nm)
0
50
100
150
Temperature (K)
Vapor-deposition
HD-ASW
LD-ASW
Matrix sublimation
MS-HDA
pure H2O
CO:H2O=10:1
CO:H2O=50:1

Fig. 6

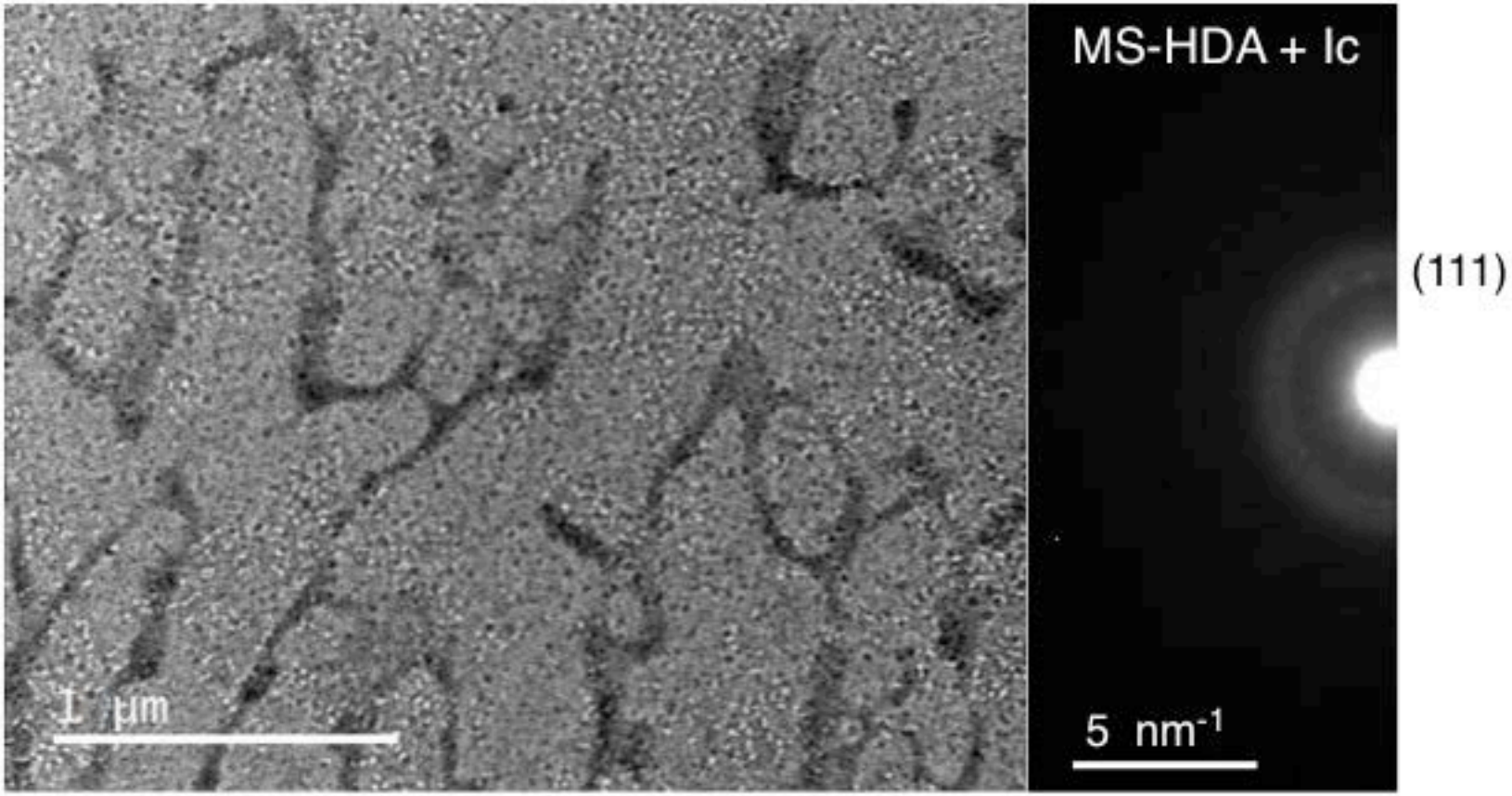

Fig. 7

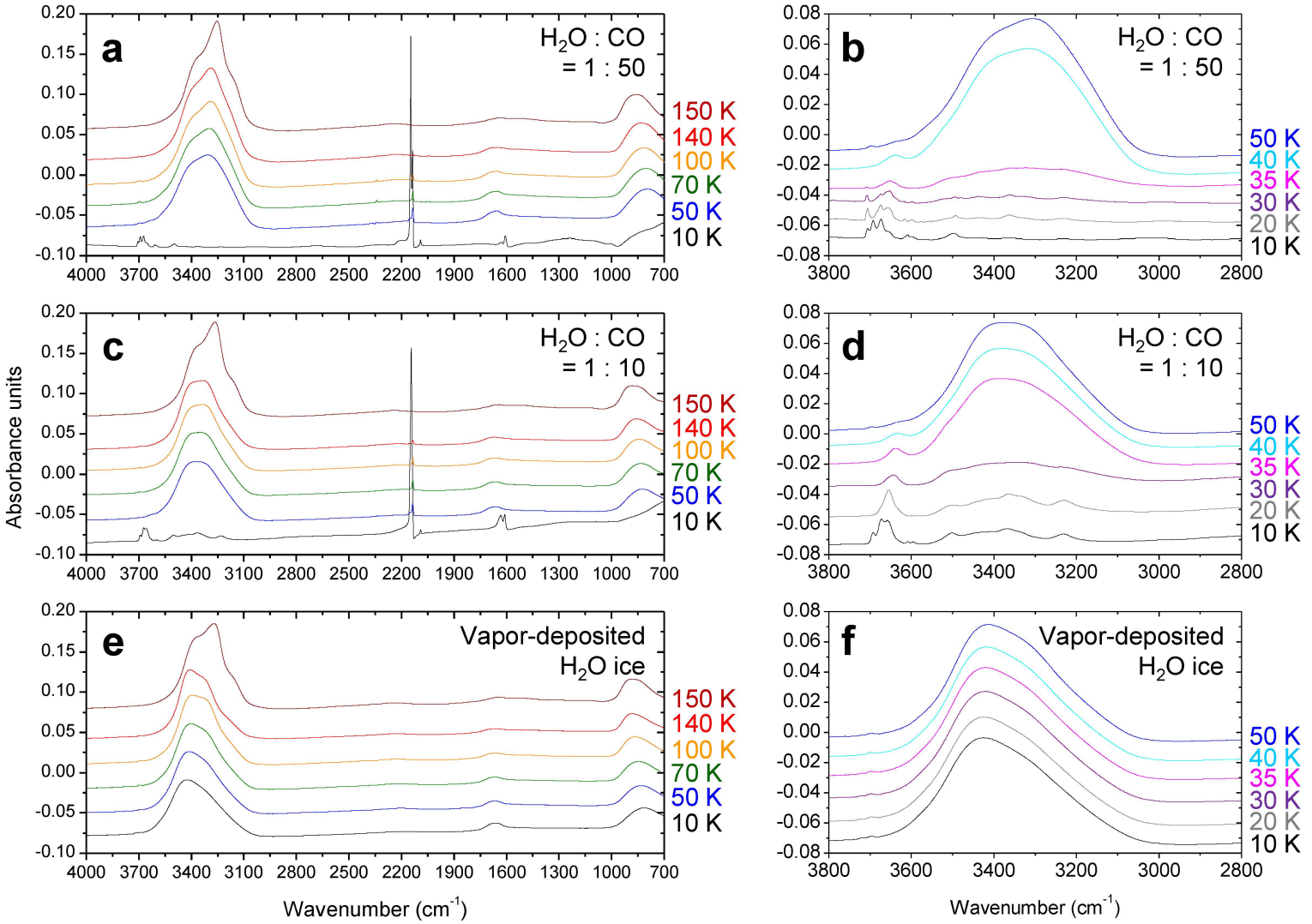
a
H2O : CO
= 1 : 50
150 K
140 K
100 K
70 K
50 K
10 K
b
H2O : CO
= 1 : 50
50 K
40 K
35 K
30 K
20 K
10 K
c
H2O : CO
= 1 : 10
150 K
140 K
100 K
70 K
50 K
10 K
d
H2O : CO
= 1 : 10
50 K
40 K
35 K
30 K
20 K
10 K
e
Vapor-deposited
H2O ice
150 K
140 K
100 K
70 K
50 K
10 K
f
Vapor-deposited
H2O ice
50 K
40 K
35 K
30 K
20 K
10 K
Absorbance units
Wavenumber (cm-1)
Wavenumber (cm-1)

Fig. 8

Supplementary-Table 1. Assignment of water clusters in CO matrix based on previous works. Symbols ν_1, and ν_3, refer to the symmetric, and the asymmetric OH stretching modes, respectively. $(CO)_m(H_2O)_n$ represents complexes of CO and H_2O.

Wavenumber (cm^{-1})	Assignment	Mode	References[1]
3707	Monomer	ν_3	[22]
3692	Monomer	ν_3 for monomeric H_2O trapped in a different matrix site.	[22]
	$(CO)_m(H_2O)_n$	ν_3	[23]
	CO-H_2O ice interface, or Dimer	OH stretching	[24]
3674	Dimer	ν_3	[22]
	$(CO)_m(H_2O)_n$	ν_3	[23]
	CO-H_2O ice interface, or Dimer	OH stretching	[24]
3658	Tetramer, Polymer	OH stretching	[22]
3640	Polymer	OH stretching	[22]
3617	Monomer	ν_1	[22]
3610	Dimer	OH stretching	[24]
3598	Dimer, Polymer	ν_1	[22]
3495	Dimer	ν_3	[22]
3438	Trimer	OH stretching	[22]

3364	Tetramer, Polymer	OH stretching	[22]
3227	Polymer	OH stretching	[22]

[1]: [22] Hagen et al. (1981), [23] Givan et al. (1996), [24] Givan et al. (1998)

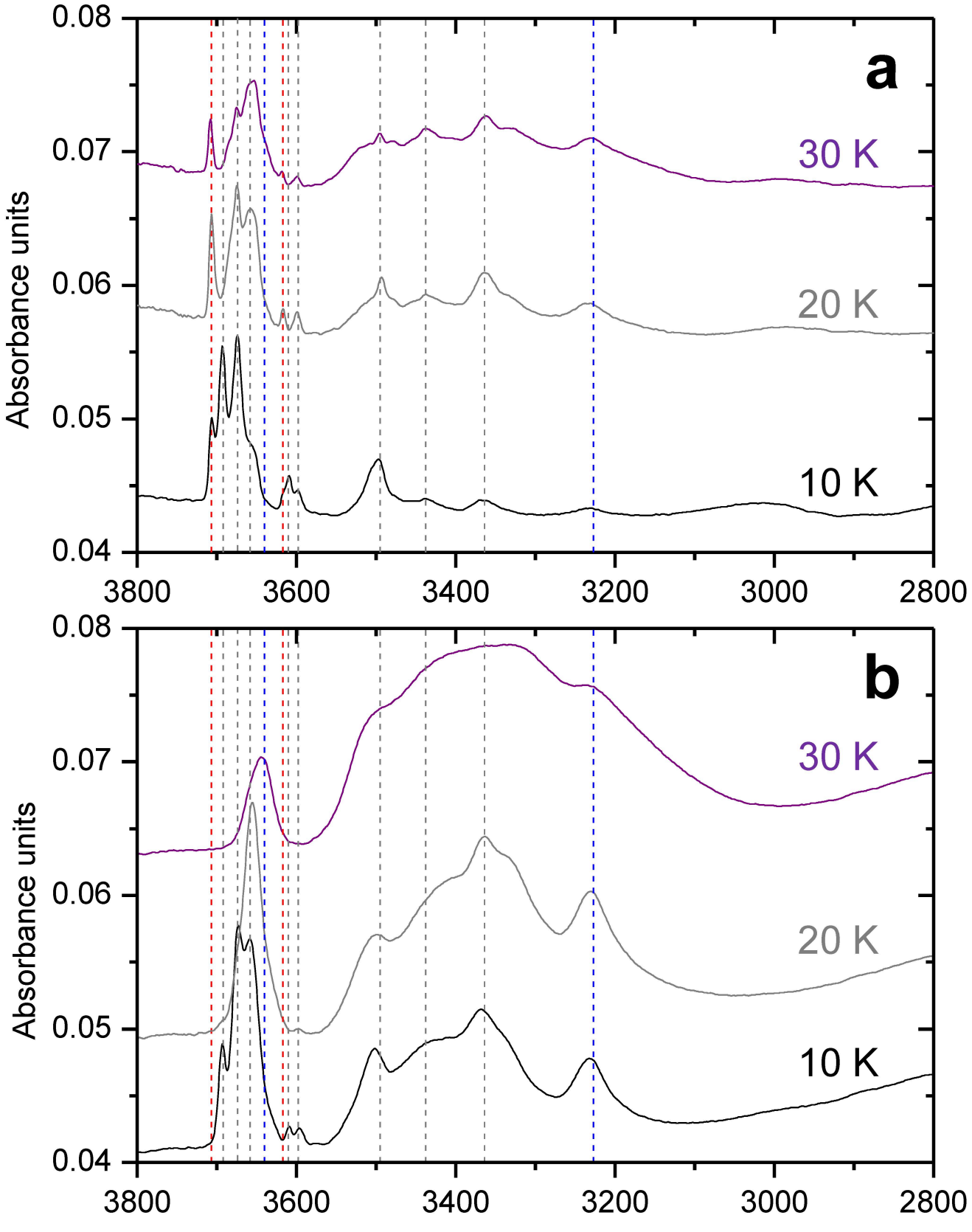
a
30 K
20 K
10 K
Absorbance units
0.08
0.07
0.06
0.05
0.04
3800
3600
3400
3200
3000
2800
b
30 K
20 K
10 K
Absorbance units
0.08
0.07
0.06
0.05
0.04
3800
3600
3400
3200
3000
2800
Wavenumber (cm-1)

SupplFig. 1

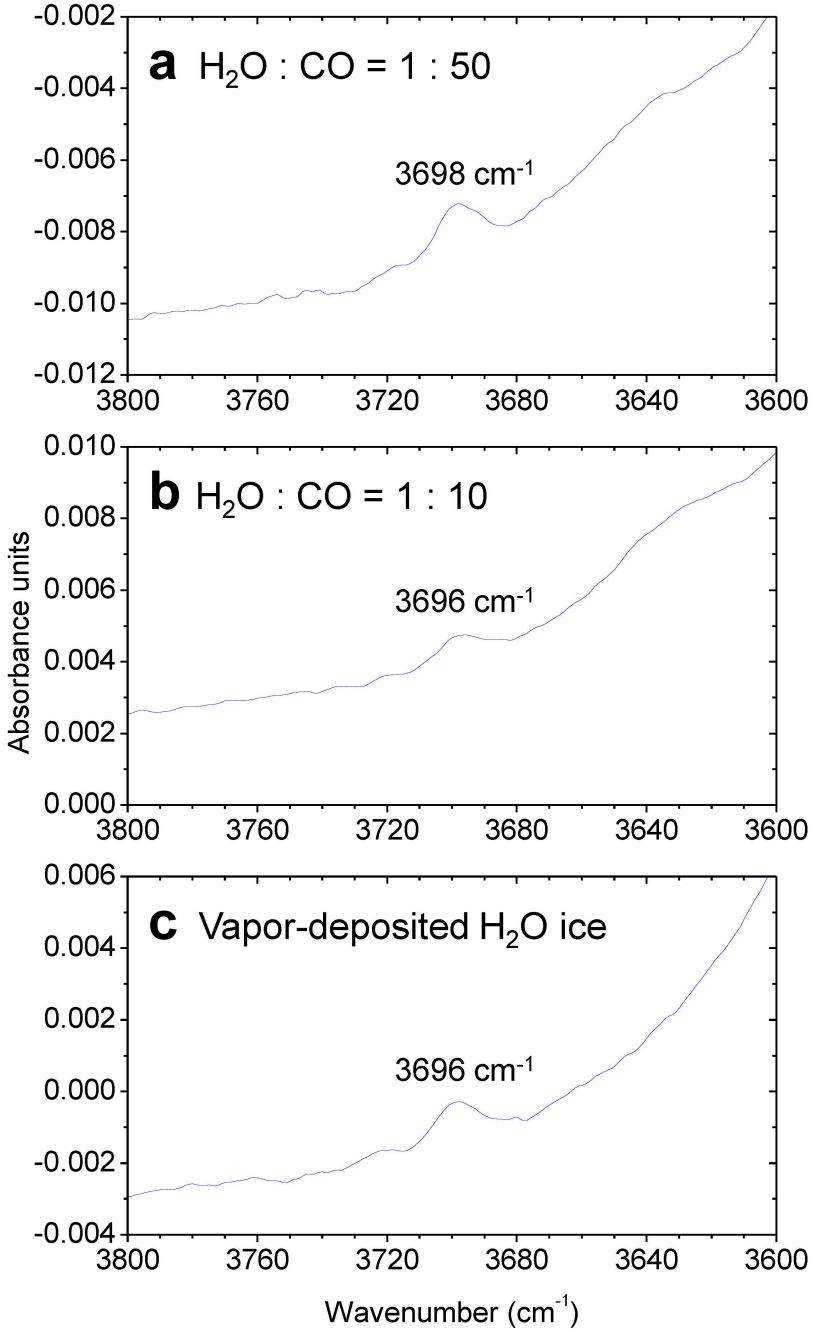
a H2O : CO = 1 : 50
3698 cm-1
b H2O : CO = 1 : 10
3696 cm-1
c Vapor-deposited H2O ice
3696 cm-1
Absorbance units
Wavenumber (cm-1)
-0.002
-0.004
-0.006
-0.008
-0.010
-0.012
0.010
0.008
0.006
0.004
0.002
0.000
-0.002
-0.004
3800
3760
3720
3680
3640
3600

Supple Fig.2

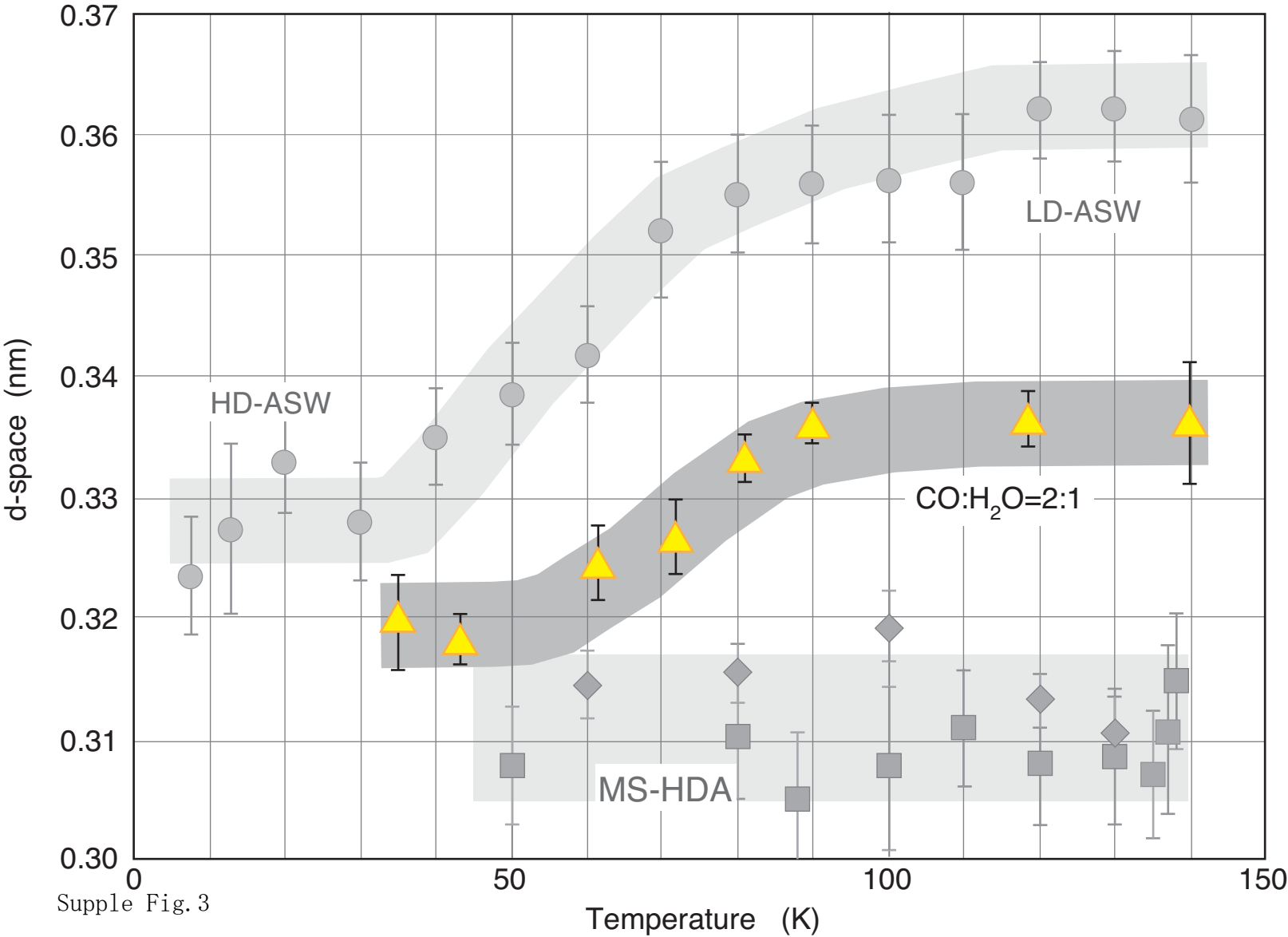
0.37
0.36
0.35
0.34
0.33
0.32
0.31
0.30
d-space (nm)
0
50
100
150
Temperature (K)
LD-ASW
HD-ASW
CO:H2O=2:1
MS-HDA

Supple Fig. 3

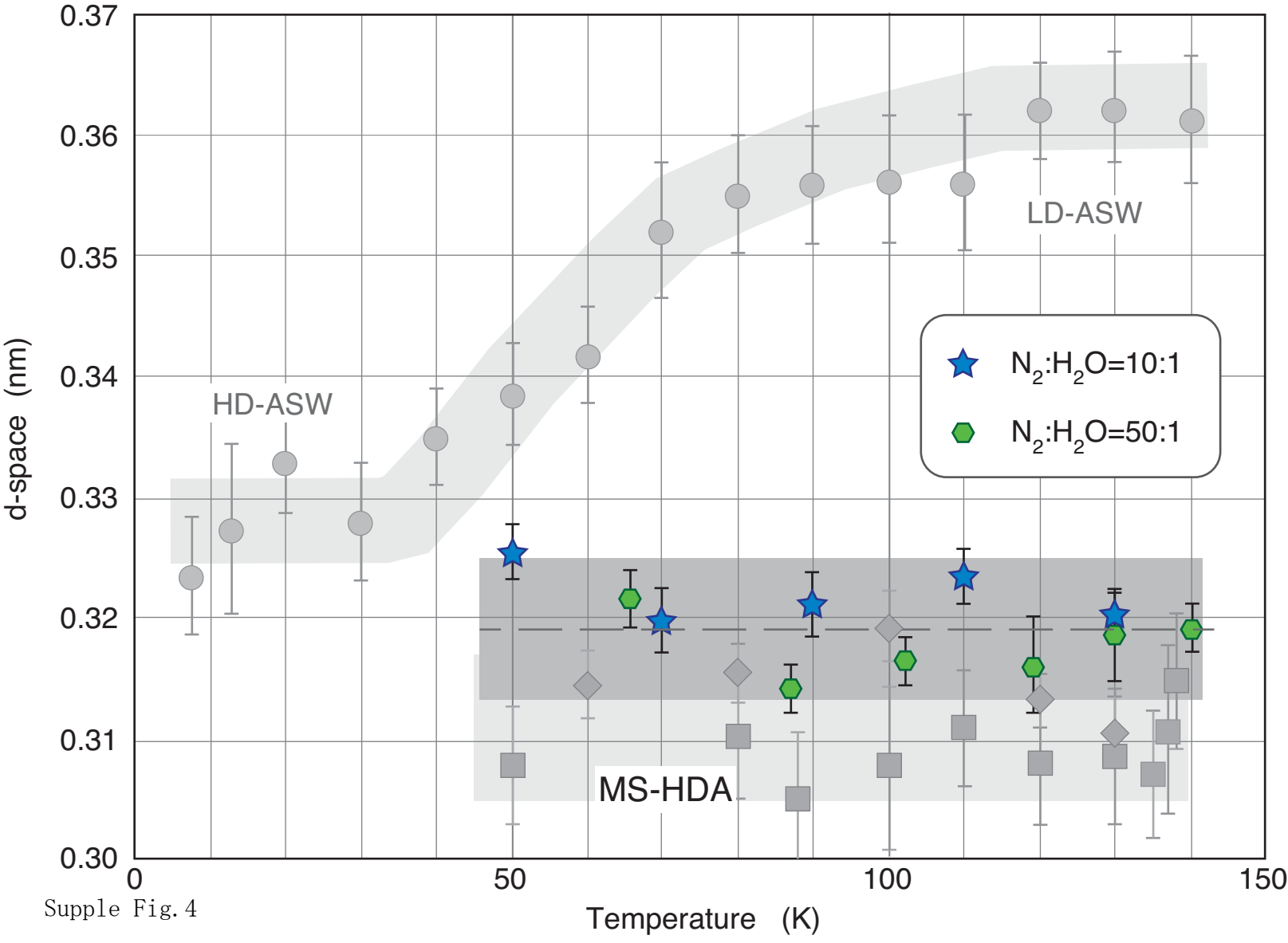
0.37
0.36
0.35
0.34
0.33
0.32
0.31
0.30
d-space (nm)
0
50
100
150
Temperature (K)
HD-ASW
LD-ASW
MS-HDA
N2:H2O=10:1
N2:H2O=50:1

Supple Fig. 4